ELSEVIER

Sensors and Actuators 83 (2000) 231–236

SENSORS AND ACTUATORS A PHYSICAL

www.elsevier.nl/locate/sna

Vaporizing liquid microthruster

E.V. Mukerjee *, A.P. Wallace, K.Y. Yan, D.W. Howard, R.L. Smith, S.D. Collins

Micro Instruments and Systems Laboratory (MISL), Department of Electrical and Computer Engineering, University of California, Davis, 1 Shields Avenue, Davis, CA, 95616, USA

Accepted 17 December 1999

Abstract

MEMS technology is expanding into increasingly diverse applications. As part of a micropropulsion system, microthruster attitude controls have been micromachined in silicon. This paper presents the microthruster design, fabrication, and test results. Fluid injected into a microchamber is vaporized by resistive silicon heaters. The exiting vapor generates the thruster force as it exits a silicon micro-nozzle. The vaporization chamber, inlet and exit nozzles were fabricated using anisotropic wet etching of silicon. With a 5 W heater input, injected water could be vaporized for input flow rates up to a maximum of 0.09 cc/s. Experimental testing produced thruster force magnitudes ranging from 0.15 mN to a maximum force output of 0.46 mN depending on fabrication parameters: chamber length, nozzle geometries, heater power, and liquid flow rates.

Keywords: Microthruster; Wafer bonding; Fluid; Spacecraft; Micromachining

1. Introduction

The production of microspacecraft [1,2] may aid NASA in decreasing launch costs, decreasing flight times, and increasing mission reliability by redundancy of spacecraft. MEMS technology is the key to the development of complex miniature instruments, mechanical components, and sensors required for microspacecraft because of its tremendous flexibility and utility. In addition, fine positioning attitude control thrusters are required on all spacecraft with stringent slew rate requirements. This paper addresses the necessity for micro-attitude control thrusters. While high-pressure gas thrusters [3,4] have been proposed they require excessive mass due to tank and supply line requirements. In the work presented, liquid fuel stored at low pressures exits the nozzle via the vaporization chamber yielding thrust, eliminating the need for high-pressure storage and confinement. While this concept has been previously proposed [3,4], the following demonstrates an efficient fabrication process and characterizes the microthruster's performance.

2. Microthruster design

A micromachined chamber is heated to vaporize a controlled liquid flow and eject the vapor for propulsion through an exit nozzle of the microthruster [5]. Two distinctly different nozzle designs were implemented: a side exit nozzle (Fig. 1) and a top exit nozzle. As shown in Fig. 1, fluid enters through an etched inlet via hole into the vaporization chamber. The heater was placed on the surface of the thruster since silicon is an excellent thermal conductor. Glass, used to seal the microchambers in the so-called asymmetrical design (Fig. 2), is a poor thermal conductor and therefore compromises heater efficiency. It was used only to provide a window for visual observation of fluid flow and vaporization within the microchamber during operation in this early development stage. Vaporization of the fuel in the microchamber has a longer pre-vaporization warm up time because heat is being delivered only to one side. However, even with the glass cover, the silicon containing diffused heaters [6] provided sufficient thermal contact and conductivity to effectively heat the microchamber. A side exit nozzle is the major benefit of this design. The nozzle in this configuration can be optimized for maximizing specific impulse. In the top exit design, the thickness of the wafer and etching technology limits nozzle geometry, especially its length. Anisotropic

* Corresponding author. Tel.: +1-530-752-4637; fax: +1-530-752-8428.

E-mail address: mukerjee@ece.ucdavis.edu (E.V. Mukerjee).

0924-4247/00/$ - see front matter
PII: S0924-4247(99)00389-1

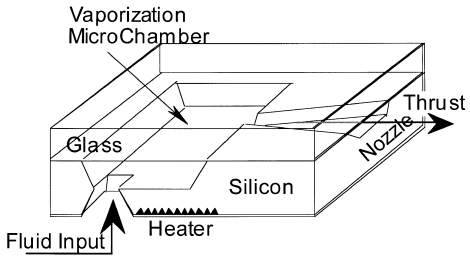

Fig. 1. Diagram of edge nozzle microthruster.

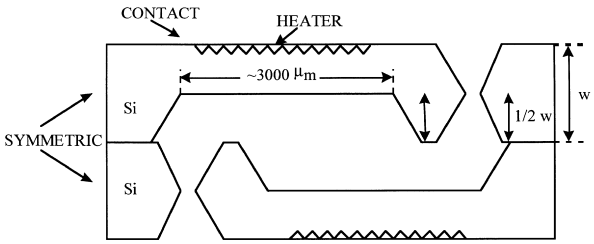

Fig. 3. Symmetrical thruster design with top nozzle exit.

etching from the wafer backside formed the fluid inlet to the chamber producing an opening on the chamber side of 50 μm. Fig. 3 illustrates a top exit nozzle design where ''identical'' wafers are silicon-to-silicon fusion bonded [7–9]. This design, being more power efficient, allows thermal input from heaters on both sides of the microchamber and utilizes the high thermal conductivity of silicon. The vaporization chamber volume is $\approx 7.5 \times 10^{-4}$ cm^3 for both microthruster designs. The size and geometry of the exit nozzle, vaporization chamber, and heater are crucial in obtaining optimal performance of linear thrust. However, development of an accurate model of these effects was beyond the scope of this preliminary investigation. Therefore, a series of different microthruster designs were fabricated to create a testbed for experimental comparison of performance. Exit nozzle flange angles (2°, 6°, 22.5°, and 45°), vaporization chamber lengths (3 and 5 mm), and three different heater geometries are variables in the testbed. Both diffused heater element designs (Fig. 4) had the same number of squares, and therefore the same total resistance ($\approx 200\ \Omega$). The third heater geometry uses silicon as the heating element; aluminum contact pads annealed directly to the bulk silicon provide the electrical connection.

3. Microfabrication

3.1. Diffused heaters

The microthrusters were fabricated in a 4 in. diameter, (100) oriented, p-type silicon wafers. Wafers were cleaned with the RCA cleaning process [10]. A thermal, wet oxidation was performed at 1000°C to produce 0.8 μm of SiO_2, which was used as a high temperature diffusion mask. Standard photolithography and oxide etching in HF were performed to open the heater patterns for diffusion of phosphorous from solid source wafers at 925°C. Junction depth was determined to be approximately 1 μm and sheet resistance was determined to be 10–11 Ω/sq. After diffusion, the masking oxide was stripped with 49% HF. Next, a thin (500 Å), stress relieving thermal oxide is thermally grown at 1000°C in dry oxygen. This was followed by deposition of 1500 Å of LPCVD silicon nitride. The heaters are created in the silicon on the side opposite the microchambers. An infrared aligner (Optical Associates) was used to perform alignment of the heaters on the backside of the wafers to the microchambers on the front side. This requires use of an IR visible alignment mark on the heater side of the substrate. Since the heater diffusions are not clearly visible, an aluminum feature was created next to the heater pattern for use in backside alignment.

3.2. Structure definition

Photoresist was next spun onto both sides of the wafers and photolithographically patterned, using the IR aligner, to transfer the microthruster chamber, nozzle and fluid inlet port patterns onto their respective sides of the wafer. The silicon nitride was then etched by reactive ion etching (RIE) in $SF_6 + O_2$, followed by wet etching in a buffered HF solution to remove the underlying oxide. The photoresist is then stripped and the exposed silicon is etched in 22 wt.% KOH/H_2O solution at 60°C to form the microchambers, nozzles and inlet holes.

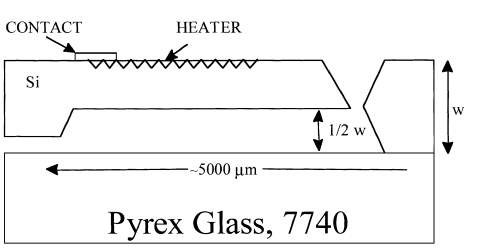

Fig. 2. Asymmetrical thruster design with side nozzle exit.

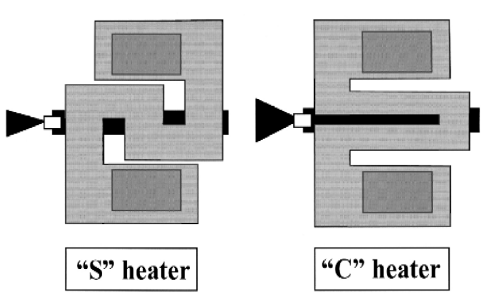

Fig. 4. Heater designs.

3.3. Bonding

3.3.1. Symmetrical design

After the KOH etch of silicon, nitride and oxide are removed with 49 wt.% HF and the wafer is cleaned by a modified RCA cleaning procedure (base clean, acid clean, base clean, no HF dip). This activates the silicon surface and prepares it for fusion bonding. Two identical wafers are aligned using the IR aligner, making use of the etched structures on the interior surfaces and IR imaging for alignment. Once aligned, the wafers are brought into intimate contact and pressed together to eliminate voids. The pair was annealed for 10 min at 1000°C in nitrogen followed by 50 min in dry oxygen.

3.3.2. Asymmetrical design

After the KOH etch of silicon, nitride and oxide are removed with 49% HF and the wafer is cleaned using the standard RCA procedure. The wafer was anodically bonded (Karl Suss Anodic Bonder SB-6) to a glass wafer (Pyrex #7740).

3.4. Shadow mask metal patterning

Shadow masking [11] was used to pattern the aluminum contact pads for making electrical connection to the diffused heaters. To facilitate alignment, matching pyramidal pits were etched into both the device and shadow mask by KOH etching. Gold balls were placed inside the pits of the device wafer so that as the shadow mask was brought into close proximity, the balls would key into the etched alignment pits of the shadow mask, aligning the two wafers. With this alignment technique, we have been able to achieve alignment accuracy of ± 5 μm [12], although for this particular application, alignment accuracies of ± 20 μm is sufficient. The wafer pair was held together with three small pieces of high vacuum/temperature tape placed along the pair edge. The pair was placed inside an e-beam evaporator (CHA) and 5000 Å of aluminum was evaporated through the shadow mask and onto the device wafer. The shadow mask was then detached; the device wafer cleaned, and the contacts were annealed in Ar + 4% H_2 at 425°C for 30 min. The individual thrusters were then diced apart and tested. For all the testing schemes, the asymmetrical, ''no heater'' microthruster design was utilized. The resistance of the silicon between the electrical contacts was 600 Ω (Fig. 5).

4. Experimental testing

Initial characterization of the microthruster was performed using water as the vaporization fluid, primarily for convenience. A peristaltic pump (Pharmacia Fine Chemicals Peristaltic Pump P-3) supplied liquid flow to the thruster through Tygon 750 μm inner diameter (ID) tubing which was attached to the thruster's liquid inlet using epoxy (J.B. Industro-Weld). The flow rate was calibrated

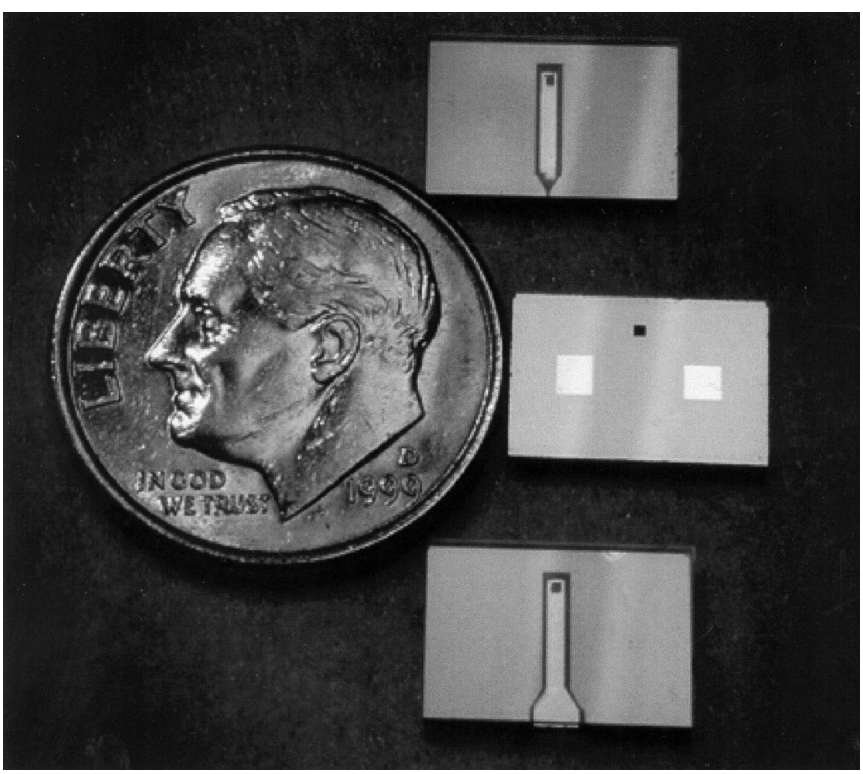

Fig. 5. Completed microthrusters.

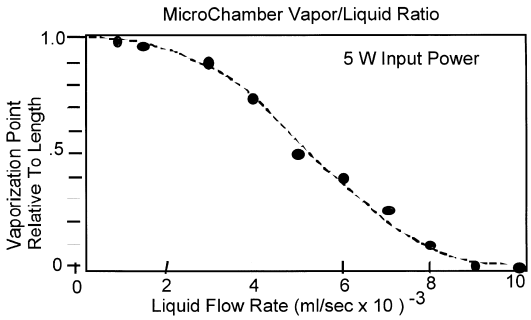

Fig. 6. Test set-up.

by filling a 1 cc syringe and dividing its volume by the total filling time. Results obtained with water are expected to be conservative relative to optimal performance results. Fluids with a lower boiling point, lower heat capacity, and lower heat of vaporization are easier to vaporize, require less power, and have higher force capability [3]. The vaporization characteristics of the side exit microthruster as a function of water flow are graphed in Fig. 6 for a constant heater input of 5 W. This data was obtained by visually observing the chamber through the glass window, varying fluid flow rate, and noting at what point along the flow path within the heated chamber vaporization occurred as measured from the outlet. It was observed that the nozzle geometry had an effect on the presence of water droplets in the output stream, but this effect has not yet been quantified.

For the next series of force measurements, Fig. 7 shows the set-up used for testing. A 1 cm section of 750 μm ID Tygon tubing is attached to the microthruster's fluid inlet via by epoxy (J.B. Industro-Weld). The tubing is then attached to a liquid supplying stainless steel needle. Electrical contact to the microthruster is made using conductive silver epoxy (Epo-tek H20E). Liquid is supplied to the thruster at a constant flow rate using a screw-driven syringe pump. The liquid flows from the syringe pump to a 500 μm ID stainless steel coil submerged in a 100°C water bath for pre-heating. Exiting the coil, the fluid enters the stainless steel inlet needle, via Tygon 750 μm ID tubing, where its temperature is further elevated to 82.5°C by resistive heating coils wrapped around the needle (measured by Omega 871 Digital Thermometer attached to the needle at the microthruster inlet point). The liquid then enters the microthruster heating chamber, vaporizes, and exits the thruster via the outlet nozzle, producing force. As shown in Fig. 7, the thruster is at one end of a rigid arm the center of which rests on a knife-edge fulcrum. The resultant thruster force was measured at the opposite end of the arm by using a calibrated microbalance with 10 μg resolution (American Scientific Products SP-182). All copper electrical wires run the length of the inlet needle and exit at the fulcrum to minimize any force contributions due to mechanical elasticity of the wires. The inlet fluid temperature, voltage and current supplied to the thruster (power), fluid flow rate and the resulting force were recorded.

5. Results

5.1. Force at constant flow and pre-heat temperature (82.5°C)

As seen in Fig. 8, the resultant force due to an increase of the heater input voltage (15 to 110 V) was measured

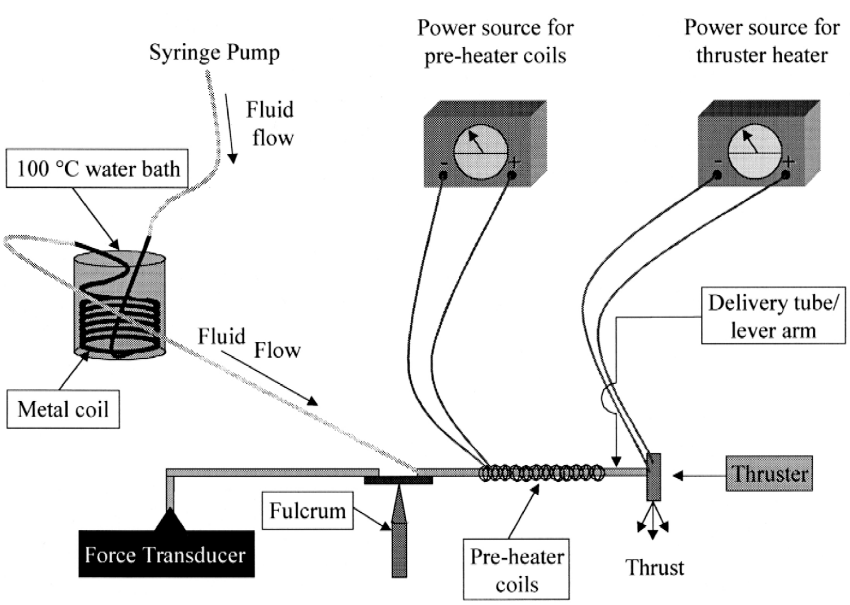

Fig. 7. Position inside chamber where water begins to vaporize (relative to total chamber length).

and found to increase rapidly with input heater power. The results shown in Figs. 8 and 9 required higher power than initial testing as reported in Fig. 6. This is due to the elimination of the insulation, reducing the inertial mass to facilitate force measurements. Maximum force at which a thrust roll off was observed was 0.31 mN. This correlates to a heater input power of 7.8 W, a flow rate of 0.21 ml/min and an inlet temperature of 82.5°C. Increasing the flow rate to 0.53 ml/min produced a greater thrust force roll off point of 0.46 mN at 10.8 W heater input power and 82.5°C inlet temperature. The increased flow rate mandated a larger temperature differential between the inlet fluid and microthruster heater to vaporize the increased mass of liquid. This is reflected as an increased heater input power to vaporization ratio. Each data point represents an average of 15 measurements. The non-zero base line reading is due to the positive force of the fluid exiting the microthruster.

5.2. Force at constant power (6.7 W) and flow (0.21 ml/min)

Original testing of the microthruster was performed using an inlet fluid temperature of 20°C (room temperature). To isolate the efficiency of the microthruster heater's ability to vaporize the fluid from the energy required to raise the temperature of the liquid to the vaporization point, the initial inlet fluid temperature was elevated. $Q_T = Q_1 + Q_2$. Q_T is the total energy required to vaporize the fluid. Q_1 is the energy required to raise the temperature of the fluid to the vaporization point. ($Q_1 = mc\Delta T$; m = mass, c = heat capacity, ΔT = vaporization temperature — initial inlet fluid temperature). Q_2 is the energy required to vaporize a liquid at the vaporization temperature. ($Q_2 = mL_V$; m = mass, L_V = latent heat of vaporization). Therefore, by minimizing ΔT, most of the energy supplied to the microthruster heater will be utilized to cause the phase change. From Fig. 9, it is shown that the average force output of the microthruster is linearly proportional to the inlet fluid temperature for a constant flow and power.

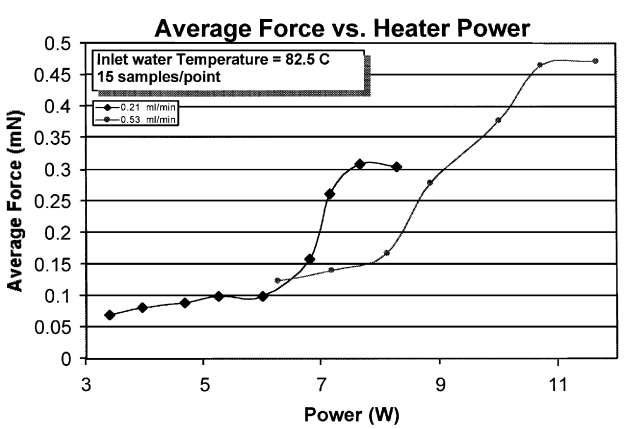

Fig. 8. Average force output for constant fluid inlet temperature (82.5°C) for two flow rates (0.21 and 0.53 ml/min).

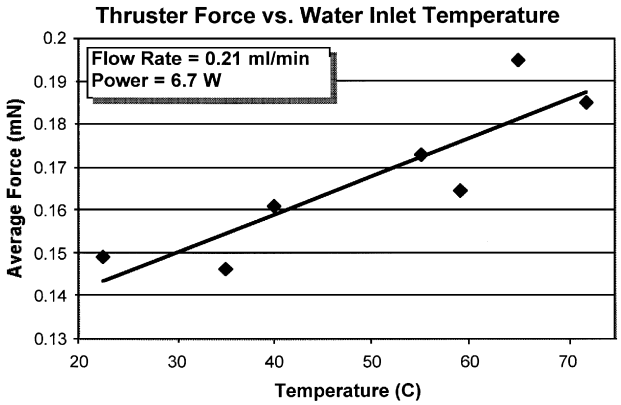

Fig. 9. Average force output for constant power (6.7 W) and flow rate (0.21 ml/min).

6. Summary

Utilizing conventional microfabrication and bonding techniques, microthrusters were designed and fabricated, and preliminary testing was performed. The thruster was demonstrated to vaporize fluid and generate thrust. Thrust measurements were obtained using modest power consumption and a high heat of vaporization fluid, water. A maximum force output of 0.46 mN at 10.8 W was observed, however, the thruster does operate at 5 W, producing sufficient thrust for its intended application of attitude control for microspacecraft. In preliminary testing of the thruster, it was observed that better vaporization occurred at lower power inputs than from subsequent experimental testing. This is a packaging issue. The microthruster was encapsulated in high temperature plexiglass chuck for vaporization testing so the thruster was thermally isolated form the environment. The force measurement set-up exposed the microthruster to air on all sides, effectively creating a heat sink, and thus requiring more power. Due to experimental limitation, powers exceeding 11 W could not be tested because of thermal breakdown of the epoxy used. Future optimization of the chamber geometry, nozzle geometry, and fuel choices will enable the thruster to produce larger forces while decreasing its power consumption. This microthruster is one component of a micropropulsion system. The presented design is relatively simple and could be readily integrated with other MEMS components such as micro-valves, fluid mixers, and fluidic interconnects [13].

Acknowledgements

This project began as a graduate laboratory course project (EEC246) at UCDavis, instructed by Professor R.

Smith. The authors wish to acknowledge the other members of the class, Carl Arft, Kimberly Cornett, Mike Guddal, Uma Krishnamoorthy, and Anne Vandooren, for their contributions to the thruster design and microfabrication. The authors also acknowledge Juergen Mueller, Bill Tang, and others of the Jet Propulsion Laboratory, whose early work on microthrusters provided the motivation for this project.

References

[1] P.K. Wang, F.Y. Hadaegh, Coordination and control of multiple microspacecraft moving in formation, Journal of the Astronautical Sciences 44 (3) (1996) 315–355.

[2] R.M. Jones, Electromagnetically launched microspacecraft for space science missions, Journal of Spacecraft and Rockets 26 (5) (1989) 338–342.

[3] J. Mueller, Thruster options for microspacecraft: a review and evaluation of existing hardware and emerging technologies, in: 33rd AIAA/ASME/SAE/ASEE Joint Propulsion Conference and Exhibit, Seattle, USA, July 6–9, 1997.

[4] J. Mueller, W. Tang, A. Wallace, W. Li, D. Bame, I. Chakraborty, R. Lawton, Design, Analysis and Fabrication of a Vaporizing Liquid Micro-Thruster, AIAA Paper 97-3054, Seattle, WA, USA, July 1997.

[5] J. Chen, K. Wise, A high-resolution silicon monolithic nozzle array for inkjet printing, in: Proceedings of the 8th International Conference on Solid-State Sensors and Actuators (Transducers '95), Stockholm, Sweden, June 25–29,1995, pp. 321–324.

[6] N. George, A. Srivastava, Design, fabrication and testing of polysilicon microheaters in silicon, SPIE 2880 (1996) 224–230.

[7] E. Klaassen, K. Petersen, J. Noworolski, J. Logan, N. Maiuf, Fabrication of SOI wafers with buried cavities using silicon fusion bonding and electrochemical etchback, Sensors and Actuators, A 54 (1996) 709–713.

[8] B. Ju, M. Oh, Fabrication of silicon membrane using fusion bonding and two step electrochemical etching-stopping, Journal of Material Science 29 (1994) 664–668.

[9] C. Gonzalez, R.L. Smith, D.G. Howitt, S.D. Collins, Microjoinery: concept, definition, and application to microsystem development, Sensors and Actuators, A 66 (1–3) (1998) 315–332, See also http://www.ece.ucdavis.edu/misl/homepage.htm.

[10] W. Kern, D.A. Puotinen, Cleaning solutions based on hydrogen peroxide for use in silicon semiconductor technology, RCA Review 31 (1970) 187–205.

[11] G.J. Burger, E.J.T. Smulders, J.W. Berenschot, T.S.J. Lammerick, J.H.J Fluitman, S. Imai, High resolution shadow mask patterning in deep holes and its application to an electrical wafer feed-through, in: Proceedings of the 8th International Conference on Solid-State Sensors and Actuators (Transducers '95), Stockholm, Sweden, June 25–29,1995, pp. 573–576.

[12] R. Garabedian, C. Gonzales, J. Richards, A. Knoesen, R. Spencer, S.D. Collins, R.L. Smith, Microfabricated surface plasmon sensing system, Sensors and Actuators, A 43 (1994) 202–207.

[13] C. Gonzalez, S.D. Collins, R.L. Smith, Fluidic interconnects for chemical analysis microsystems, Sensors and Actuators, B 49 (1998) 40–45.